

Alkali Promotion in the Formation of CH₄ from CO₂ and Renewably Produced H₂ over Supported Ni Catalysts

Charlotte Vogt^{+, [a]}, Jochem Wijten^{+, [a]}, Chantal Leal Madeira,^[a] Oscar Kerkenaar,^[a]
Kangming Xu,^[b] Rupert Holzinger,^[b] Matteo Monai^{+, [a]} and Bert M. Weckhuysen^{*, [a]}

In Power-to-Methane (PtM) plants, the renewable electricity supply can be stabilized by using green electrons to produce H₂ via H₂O electrolysis, which is subsequently used to hydrogenate CO₂ into CH₄. In this work PtM is studied in a cascade fashion, from simulated solar light to methane production in an all-in-one setup, which was newly developed for this work. This setup was used to assess the effects of H₂ stream purity on the activity of Ni/SiO₂ catalysts in CO₂ methanation. An activity effect in downstream methanation is shown to be onset by aerosols that evolve from the electrochemical splitting of water. Small amounts of K are shown to affect CH₄ production positively, but only if they are deposited in situ, via KOH aerosols. K-doped Ni/SiO₂ catalysts prepared in an ex situ manner, by impregnation with a KOH solution, showed a decrease in activity, while the

same amount of KOH was deposited. Operando FT-IR spectroscopy reveals that increased back-donation to CO-containing intermediates and carbonates formation likely causes catalyst deactivation in ex situ samples as often reported in literature for Ni/SiO₂ catalysts. The mechanism for in situ promotion is either an increased rate in the hydrogenation of CH_x (X=0–3) fragments, or a more facile water formation or desorption as CO-containing reaction intermediates are unaffected by in situ promotion. These results are relevant to PtM from a fundamental standpoint explaining the effect of potassium on nickel methanation, but also from a practical standpoint as the presented effect of in situ promotion is difficult to achieve via standard synthesis methods.

Introduction

The cascade synthesis of CH₄ from solar light (*i.e.*, Power-to-Methane, PtM) is an attractive concept that will allow us to decrease CO₂ emissions, simultaneously demodulating the mismatch in renewable electricity demand and supply and stabilizing the electricity grid.^[1,2] In the PtM concept first renewably produced electrons are used to split H₂O into H₂ and O₂. While this renewable H₂ can, in theory, be used as an energy buffer, storing H₂ is approximately an order of magnitude more costly than storing CH₄, and thus particularly for long-term (seasonal) storage of electricity, is not necessarily cost-efficient.^[3] Hence the conversion of this H₂ into CH₄ (also called


e-gas), which can be stored safely in large quantities through infrastructure that already exists, becomes interesting from an economic standpoint.^[3–6] Furthermore, methanation is already a crucial element of any engineering solution involving on-site H₂ production through low-temperature catalytic reforming of organic substrates (e.g. alcohols, formic acid).^[7]


To the best of our knowledge, at the time of writing, the Audi e-gas plant in Wertle, Germany is the largest commercial methanation plant worldwide and produces methane starting from CO₂ captured from close by produced biogas via amine scrubbing, and from H₂ generated by three 2 MW KOH-based alkaline electrolyzers powered by renewable energy. In this plant, the hydrogen produced from the electrolysis is filtered to eliminate KOH aerosols, and subsequently dehydrated and compressed to 10 bar to be stored in a buffer tank worth 1 h of methanator operation, decoupling the operation between the electrolyzer and the methanator units. The produced methane is dried and fed into the natural gas grid. Water is cycled back in the electrolyzers, while oxygen produced at the anode of the electrolyzer is vented out. The methanation reactor is cooled by molten salts and the heat is used to regenerate the amine scrubber, bringing the process efficiency from 54% (without heat recovery) to 72%.^[3] Despite the high efficiency, the process is not yet profitable, mainly due to electricity costs and fees, showcasing how cheap electricity, but also policies can play a big role for the commercialization of PtM technologies. As described for the operating PtM plant above, several important steps occur for the application of this PtM process, which are illustrated separately in Figure 1A. Solar light is first converted into electrons *via* photovoltaics (step 1). Then, these green electrons are converted into H₂ via electrolysis of H₂O (step 2,

[a] C. Vogt,⁺ J. Wijten,⁺ C. L. Madeira, O. Kerkenaar, Dr. M. Monai,⁺
Prof. B. M. Weckhuysen
Inorganic Chemistry and Catalysis group
Debye Institute for Nanomaterials Science
Utrecht University
Universiteitsweg 99
3584 CG Utrecht (The Netherlands)
E-mail: B.M.Weckhuysen@uu.nl

[b] Dr. K. Xu, Dr. R. Holzinger
Institute for Marine and Atmospheric Research (IMAU)
Department of Physics
Utrecht University
Princetonplein 5
3584 CC Utrecht (The Netherlands)

[⁺] These authors contributed equally to this work.

 Supporting information for this article is available on the WWW under <https://doi.org/10.1002/cctc.202000327>

 © 2020 The Authors. Published by Wiley-VCH Verlag GmbH & Co. KGaA. This is an open access article under the terms of the Creative Commons Attribution License, which permits use, distribution and reproduction in any medium, provided the original work is properly cited.

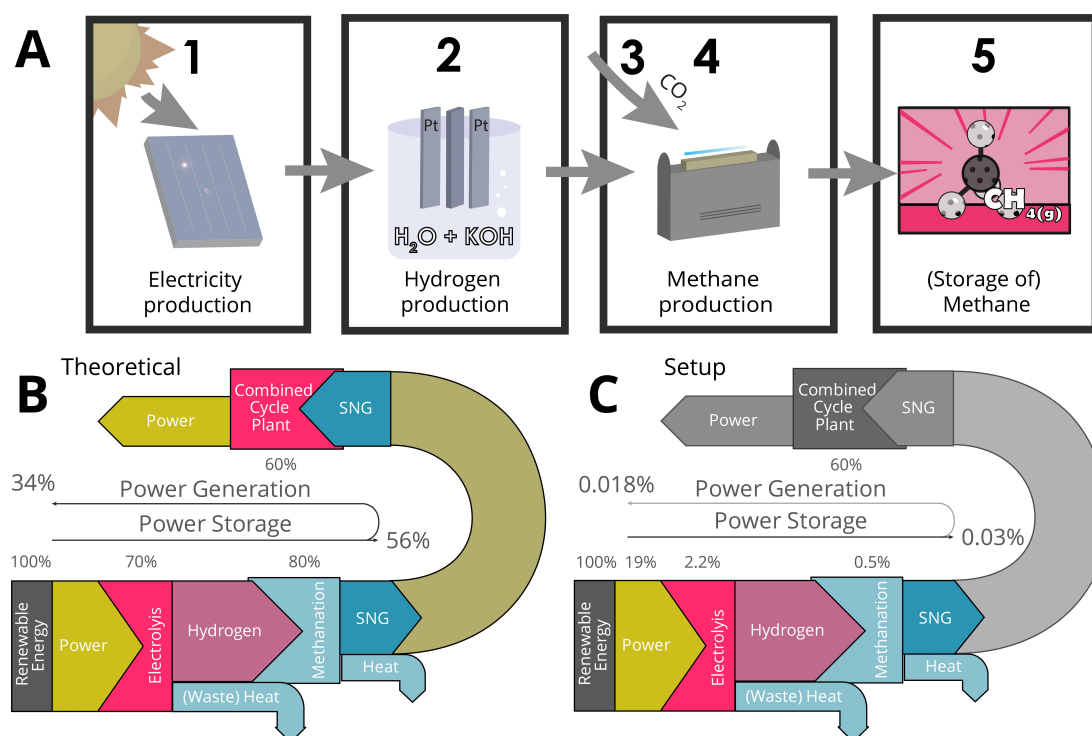


Figure 1. A) Overview of the sequence of steps in the Power-to-Methane (PtM) concept, and schematic showing B) the theoretical process efficiency of the Power-to-Methane (PtM) concept, and C) the achieved output on our non-optimized laboratory scale setup.

both the Hydrogen Evolution Reaction (HER) and Oxygen Evolution Reaction (OER) have to be considered here).^[8,9] CO₂ streams are captured and purified (step 3), and can then be converted into CH₄ via renewably made H₂ (step 4 in Figure 1). This CH₄ is then stored and distributed (within a closed-cycle process, step 5).

CO₂ reduction to methane may be regarded as an established process as French chemist Paul Sabatier (1845–1941) discovered the reaction over 100 years ago.^[10,11] Nevertheless, there are novel questions that arise from the application of this process within the concept of electrification of the chemical industry described above. An obvious question is that of the effect of sequential process steps on one another. To study such questions in detail, a setup was built bringing together all elements of this process in a single, newly constructed experimental setup, combining simulated solar light with an electrolyzer to split water, and a methanation unit. Photographs of this setup can be seen in Figure S1.

The overall process efficiency of the PtM process is highlighted in Figure 1B,C. Figure 1B highlights the theoretical values of power storage (56%) and subsequent power generation (36%), as calculated for an optimized production plant. In Figure 1C we highlight the all-in-one setup, developed in our laboratory, that will be discussed in this work and is shown in Figure S1. The yields of each step in our (non-optimized) lab-scale setup are shown in Figure 1C. Obviously, the setup that we will discuss in this work is far from what an optimized industrial plant would be, mainly due to electrode size constraints and inefficient heating of the methanation reactor,

but also because the kinetic conditions applied (*i.e.* low CO₂ conversion) were purposely chosen for the final catalytic methanation step to study activity trends. The applied setup has an overall efficiency of 0.018%. As a comparison, the theoretical maximum efficiency for photosynthesis is 11%. However, most plants yield an efficiency of approximately 0.1–3% as plants do not absorb all incoming radiation.^[12] Although the comparison between our setup and natural photosynthesis is not entirely fair, as plants convert CO₂ generally into much more useful or valuable, complex carbohydrates, it illustrates the efficiency of nature in a process that has been optimized over hundreds of millions of years.

In this work we examine the effect of hydrogen production (step 2 in Figure 1A) on methane production (step 4 in Figure 1A). More specifically, it is interesting to consider the possible presence of aerosols in the H₂ feed, which may evolve from the HER in alkaline medium. This should be done, as NASA literature from 1974 already reports the possible presence of aerosols in the feed of electrolysis systems,^[13] and industrially often aerosol filters are applied as mentioned above.

The water splitting reaction is performed in alkaline media, as the kinetically limiting step in the electrolysis of water – the OER – benefits from a high pH.^[14] Hence the aerosols that may be present in the gas feed from the split water may contain alkaline material. Literature shows both promoting, and deactivating effects for the addition of alkaline dopants to thermocatalytic methanation reactions,^[15–23] and relevant reaction steps thereof, such as the Reverse Water-Gas Shift (RWGS) reaction. Table S1 lists some of this relevant literature, and their

normalized promotional or deactivating effect on the turnover frequency of CO and CO₂ methanation. In general, alkali promoters (most commonly potassium) are added to methanation catalysts either to poison support acidity, or to catalyze coke removal via hydrogen or steam reactions.^[15] Xu et al. show a “volcano-shape-curve” between the Mg/Al molar ratio and catalytic activity, explained by an optimal surface basicity induced by the Mg.^[19] The activity and selectivity of K promoted nickel catalysts seem to mainly depend on the support.^[20] On Ni/Al₂O₃ a promotional effect is found, whereas on Ni/SiO₂, an exponential decrease in total activity with increased promoter concentration is seen which is claimed not to be due to a decrease in the dispersion.^[20] Campbell et al. also note an increase in activity for Al₂O₃-supported Ni, but a decrease in activity for SiO₂ supported Ni.^[23] While Huang et al. find a promotional effect for Ni/SiO₂.^[15] Thus, fundamentally understanding the nature of this potential promotional effect is of direct practical and academic relevance.

In this work we will study the effect of K promotion on Ni/SiO₂ catalysts of different mean nickel particle sizes, as well as different forms of addition of K to the Ni/SiO₂ catalysts via *operando* FT-IR spectroscopy, and the use of XRD, STEM-EDX and ICP-AES. To the best of our knowledge, no systematic study has been performed to distinguish the possible particle-size dependent effect of alkali promotion, while it seems a relevant variable in Table S1, and no study has considered the effect of *in situ* deposition of potassium onto a Ni-based methanation catalyst as a potential promoter.

Experimental

Catalyst materials

Table 1 lists an overview of the fresh, or “parent” Ni/SiO₂ catalyst samples that are studied in this work.

The Supporting information (e.g. Table S2), and previous literature^[24] gives more information on the characterization of these materials. The effect of *in situ* doping with KOH-containing aerosols which evolve from hydrogen production on the catalyst samples listed in Table 1 was compared to an *ex situ* doping procedure where a 0.6 wt% K loading was achieved by impregnation, via suspension of the catalyst materials in a KOH solution and subsequent evaporation.

Table 1. Characteristics of the set of well-defined Ni/SiO₂ catalysts (1–6), listing their Ni mean particle sizes after reduction, and their Ni weight loading. Table S2 in the Supporting information lists more details on the characterization.

Catalyst sample code	Particle size after reduction [nm]	Ni weight loading [%]
1	1.2 ± 0.5	4.7
2	1.4 ± 1.4	5.0
3	2.0 ± 0.8	6.7
4	2.1 ± 1.1	11.8
5	4.4 ± 2.4	19.5
6	6.0 ± 1.9	60.0

Hydrogen production via electrolysis and cascade methanation reaction

Pt mesh electrodes (MaTecK, 99.9%, 25 × 50 mm, 3600 mesh/cm², 0.04 mm wire diameter) interwoven with a Pt wire (MaTecK, 99.9%, 1 mm diameter, 100 mm length) were suspended in a 1 M KOH electrolyte (ACS reagent, > 85% pure, ~15% water) loaded into a homemade H-cell. This cell consists of GL14 glass tubes with an internal volume of 20 mL for the electrolyte on each side, resulting in 40 mL electrolyte in total. The HER and OER reactions are spatially separated by a Nafion 117 perfluorinated membrane (Aldrich, 0.007 in. thick). Prior to use the membrane is activated by immersion in nitric acid for several hours, while the Pt electrodes were cleaned by using a butane flame. The electrolyte was purged with 2 mL/min Ar, 0.1 mL/min Kr on the HER side and 2 mL/min N₂, 0.1 mL/min Kr on the OER side for at least 2 h prior to the experiments.

The Ni/SiO₂ catalysts (3 mg, sieve fraction 75–150 μm) were loaded in a plug-flow reactor (borosilicate capillary, 1 mm diameter) and reduced at 550 °C for 60 min, with a heating rate of 5 °C/min under a flow of 1 mL/min of pure H₂. Afterwards, the catalysts were cooled down to 400 °C (5 °C/min) under a flow of pure N₂. This flow was maintained for 3 h to remove residual H₂ from the system.

Electrochemistry (Ivium CompactStat) was then started potentiometrically at a current of 4 mA, requiring ca. 1.69 V potential (the Nafion membrane yields a high resistance in the system), 1.69 V also being the output of a small solar cell module of three cells in series. See also Figure S3 for chronopotentiometry of the water splitting with two Pt electrodes, and the GC response to the application of current. The flow of Ar/Kr and N₂/Kr was constantly maintained as a carrier gas for the produced H₂ and O₂. The feed from the HER was led over the plug flow reactor containing the Ni/SiO₂ catalyst, optionally filtered by an aerosol filter.

After 15 min of flow from the H-cell an 800 ppm CO₂ feed was opened over the Plug Flow Reactor (PFR) at a rate of 1 mL/min and was mixed with the HER feed prior to injection on the PFR. The reactor output gas was again filtered by an aerosol filter before being injected on an InterScience CompactGC every 4 min and analyzed by FID. The flow was split over two column systems optimized for measure hydrocarbons on one end and CO/CO₂/CH₄ on the other. The latter was equipped with a methanizer to visualize each component. On a separate channel the flow from the oxygen halve of the system was injected and measured by a TCD every 4 min. This state was maintained for several hours, up to 2 or 3 days depending on the experiment.

Aerosol measurement and formation

To measure the aerosol formation from the electrochemical cell, a Water-based Condensation Particle Counter (WCPC, TSI model 3785) was attached to the output of the cell, in place of the methanation reactor. This is shown in Figure S2. In a typical experiment, a 2 mL/min flow of N₂ was bubbled through the electrochemical cell filled with 1 M KOH, and the outlet stream was diluted with 1 L/min filtered air before being fed to the particle counter. The effect of flow, applied potential and KOH concentration was also studied, see Figure S4. Control experiments carried out bypassing the cell or using water instead of 1 M KOH didn't show any aerosol formation.

Operando FT-IR spectroscopy with on-line gas chromatography

Operando FT-IR spectroscopy was performed using a Bruker Tensor 37 FT-IR spectrometer and OPUS software with DTGS detector.^[24] Spectra were recorded every 30 s. Gases were introduced with Brooks mass flow controllers. Self-supported catalyst wafers for *operando* transmission FT-IR spectroscopy were prepared using roughly 4 tons of pressure. The catalyst wafers (15 mg in weight) were loaded into a Specac high-temperature transmission FT-IR reaction cell, and subsequent *in situ* reduction was performed with 1:1 H₂:N₂ flow of 20 mL/min each for 1 h at 550 °C. Temperature increased at a rate of 5 °C/min and atmospheric pressure was held throughout. The cell was cooled to 100 °C before CO₂ hydrogenation commenced, after which temperature was increased at 5 °C/min to 400 °C where it was held for an hour. Gas rates used in CO₂ hydrogenation without water were 6.25 mL/min N₂, 5.00 mL/min H₂, and 1.25 mL/min CO₂. For experiments with water in the gas feed, water was fed through a stainless steel saturator, by bubbling inert gas. Milli-Q water was fed at 21 °C, which at 6.00 mL/min N₂ ensured 2.8% (or 0.36 mL/min) was added to a feed of, 5.00 mL/min H₂, and 1.25 mL/min CO₂. *Operando* FT-IR experiments were performed at atmospheric pressure, with online gas chromatography. Global Analyst Solutions CompactGC 4.0 and Thermo Scientific Dionex Chromeleon 7 software were used for online gas chromatography, with FID and TCD detectors. Product and transients continued to be captured for 15 min after CO₂ and 5 min water saturator was closed until H₂ was closed, all while at 400 °C.

KOH aerosol semi-quantitative characterization

The Ni/SiO₂ catalysts tested for up to 3 days in the methanation reaction using the H₂ produced by the HER showed a content of 0.6 ± 0.2 wt.% K by ICP-AES analysis. Assuming that all K from the gas feed gets adsorbed on the catalyst, this would give a value of 4–11 µg/L KOH (4 mg of sample, 2 mL/min gas carrier flow). Comparable to the KOH content reported by NASA (3–5 µg/L).^[13] Considering pure KOH density (2.12 g/mL) we can calculate the volume (in mL) of KOH per mL: ~2–5 × 10⁻⁹. Which, divided by the observed number of particles (about 30 per mL in the flow analyzed in the counter, which is diluted 500 times with N₂, corresponding to 15000 per mL in the starting 2 mL flow), gives a volume per particle of ~0.3–0.6 × 10⁻¹² mL, *i.e.* ~0.3–0.6 µm³. Assuming a spherical shape, this corresponds to 0.4–0.5 µm radius, ~1 µm diameter.^[25]

Setup efficiency calculation

The Solar Simulator used is a Sol3 A Class AAA, IEC/JIS/ASTM, 450 W Xenon, 4 × 4 inch Newport 94043 A solar simulator. It has an output of 100 mW/cm² light with a 104.04 cm² light spot. A solar module of 4 solar cells was put together, and was of a size that the entire light spot fell on the solar cells. The solar simulator output was 104.04 × 100 = 10.4 W. The solar cells had a measured output of 2.44 V and 0.832 A and thus had an output of 2.03 W. Thus, the efficiency of this first step was 19.5%.

Due to size constraints, at 2.44 V our Pt electrodes only allow a current of 38.49 mA. At this current a Faradaic Efficiency (FE) of 100% would yield 0.268 mL/min of hydrogen. However, we measure 0.253 mL/min so the F.E. at 2.44 V is 94.4%. This means that, assuming perfect oxidation, 44.7 mW of H₂ was produced. So, the energy storage efficiency was 2.2% in the electrolysis system. With optimization it could be 5.797 mL/min of H₂, which corresponds to 0.966 W H₂ and thus an energy efficiency of 47.6%. The corresponding Solar-to-Hydrogen (StH) is 0.43% in the system, or 9.28% with optimization.

The heater of the plug flow reactor is operated at 19 V and 3.5 A, and thus consumes 66.5 W. Taking the hydrogen into account the energy input is 66.5447 W. 3% of the CO₂ is converted, 0.5% into CH₄ (0.03 mL/min) and 2.5% into CO. Considering only CH₄ and its energy density of 55.5 MW·s/kg that means the energy stored in CH₄ is: 0.0199 W. This means the energy efficiency of the entire step is 0.03%, which is mainly due to the inefficient heating. See Table 2, or Figure 1A for an overview.

Results and Discussion

We have studied a set of SiO₂ supported nickel catalysts, labelled from 1–6 in accordance with increasing particle size (see also Table 1). Previous literature^[24] lists full details on the catalyst samples, which were characterized by several techniques such as H₂ chemisorption, N₂ physisorption, HAADF-STEM, temperature programmed reduction, X-ray absorption spectroscopy. A benchmark 1 M KOH alkaline solution is used for the production of renewable H₂ via H₂O electrolysis,^[14,26] and we focus on its effect on the catalytic hydrogenation of CO₂ into CH₄ over the mentioned catalyst samples.

H₂O splitting to H₂ and O₂ was performed with two Pt electrodes and done in a stable manner at 1.69 V at a current of 4 mA. O₂ production was used to control the water splitting efficiency, and was stable at a Faradaic efficiency of 99.6% (Figure S3). By use of a H₂O-based condensation particle counter, which is shown in Figure S2, the presence of aerosols could be detected in the HER-produced H₂ feed. The concentration of aerosols formed is shown in Figure 2A. Figure 2B shows that the hydrogen produced by electrolysis has an effect on the activity of the sample shown (catalyst sample 5 in Table 1). More specifically, the H₂ produced via electrolysis, seemed to have a promoting effect on the activity of the Ni/SiO₂ catalyst in CO₂ methanation at 400 °C and ambient pressure, as shown in Figure 2B, when compared to clean hydrogen from the bottle under the same reaction conditions.

In Figure 3, the effect of the H₂ from HER on different Ni/SiO₂ catalyst samples with varying mean nickel particle sizes is shown, as tested in the all-in-one setup. The investigated Ni/SiO₂ catalysts show stable methanation activity at 400 °C, over a prolonged period of time when pure H₂ from a cylinder is used as a feedstock, but this changes when H₂ from the HER is used. The observed turnover frequency (TOF) values using “clean” hydrogen in this setup are comparable to previously shown results, which were measured in a different setup, an *operando*

Table 2. Summary of energy input and output of each of the three steps with the energy efficiency per step as well as the total efficiency in the last column.

Step	Input [W]	Output [W]	Energy efficiency [%]	Total efficiency [%]
Solar Cells	10.4	2.03	19.5	19.5
Electrolysis	2.03	0.0447 (H ₂)	2.2	0.43
CO ₂ hydrogenation	66.5447	0.0199 (CH ₄)	0.03	1.3 × 10 ⁻⁴

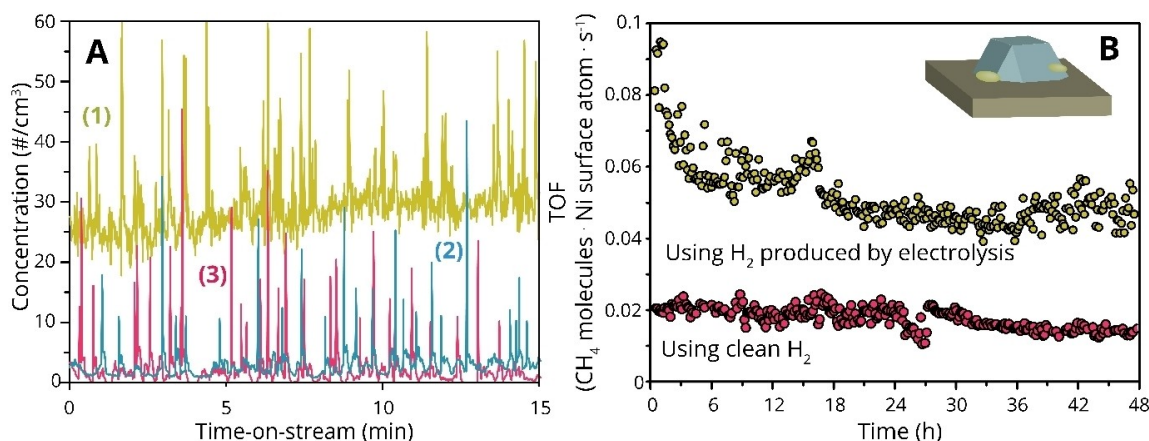


Figure 2. A) Concentration of aerosols measured via a H₂O-based condensation particle counter in the gas feed from a KOH solution in which hydrogen evolution reaction (HER) is performed, in the absence (yellow line, 1) and in the presence (blue line, 2) of an aerosol filter. The concentration observed when the electrochemical cell is bypassed is shown in pink (3). B) Trends in the methanation reaction using clean H₂, and unfiltered H₂ produced via the HER in alkaline medium for 2 days run time, CH₄ activity is indicated by TOF values are shown at 400 °C, over a Ni/SiO₂ catalyst with 4.4 nm mean particle size. Upper right corner of B) shows schematic of K promotion via *in situ* deposition on and around supported nickel nanoparticles. Conditions: 400 ppm CO₂, 9600 ppm H₂, N₂ balance, GHSV 30,000 h⁻¹.

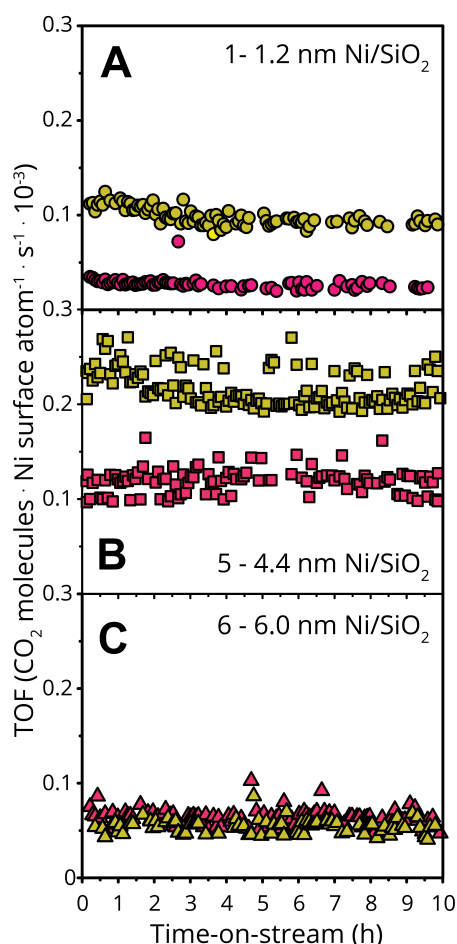


Figure 3. 10 h trends in the methanation reaction CO₂ TOF at 400 °C over Ni/SiO₂ catalyst of A) 1.2 nm, B) 4.4 nm and C) 6.0 nm mean nanoparticle size (corresponding to catalyst samples 1, 5, and 6), using H₂ from a cylinder (pink dots) or from the HER reaction (yellow dots). Conditions: 400 ppm CO₂, 9600 ppm H₂, N₂ balance, GHSV 30,000 h⁻¹.

FT-IR spectroscopy setup.^[24] Additional activity data is given in Figures S5–S8.

Interestingly, when the reaction proceeds with H₂ produced via the HER, *i.e.* with alkaline aerosols, some trends are observed for catalysts with different mean nickel metal nanoparticle sizes. Over catalyst sample 5, which has 4.4 nm mean nickel particle size diameter supported on SiO₂, a strong transient increase in methanation activity is observed, followed by a decay in activity over time, which nonetheless remains considerably higher than the values observed using pure H₂ (Figure 3 middle). On the other hand, over larger nickel metal nanoparticles (*i.e.*, catalyst 6, 6.0 nm mean nickel particle size), no promotion is observed and the catalyst steadily deactivates over time (Figure 3, bottom). The smallest mean nickel metal nanoparticle size under study, catalyst 1, 1.2 nm Ni/SiO₂, shows increased activity as well (Figure 3, top) but less than catalyst 5 sample.

Figure 2A also shows that when a filter is placed before the methanation reactor, the aerosol can be effectively removed from the H₂ stream. In order to rule out a possible direct effect of the aerosol on the catalytic activity, *e.g.* by reaction with CO₂ in the gas-phase leading to carbonate formation (which is known to occur in mere seconds in the case of NaOH^[27]), an aerosol filter was installed on a by-pass between the electrochemical cell and the methanation unit (before the CO₂ feed), and the H₂ feed was switched from unfiltered to filtered during the reaction. Notably, the activity promotion on catalyst 5 (4.4 nm Ni/SiO₂) was maintained, which strongly suggests that the aerosol itself does not play an active role in the activity enhancement, which therefore will be solely due to K deposition on the catalyst. Strikingly, this also means that one can dose just the right amount of KOH to promote methanation activity and then remove the aerosol at will, to avoid further K accumulation, which will eventually be detrimental to the activity.

In these experiments, TOF values are proportional to activity as the particle size distribution does not change significantly for the spent catalysts using filtered ("clean") H₂, and unfiltered H₂ (containing aerosols), as shown by TEM analysis in Figures S8–S10. Quite obviously, impurities in the H₂ feed from HER have an effect on the downstream catalytic methanation reaction. As a result, 0.6 ± 0.2 wt.% K was observed by ICP-AES analysis of the Ni/SiO₂ catalysts after 2 days of reaction when using HER-produced H₂, while on the undoped sample, and the catalyst tested with pure H₂ K amount was below the detection limit. These values correspond to expected KOH concentrations with respect to aerosol particle sizes in accordance with literature (4–11 µg/L KOH, 1 µm diameter particles, see the experimental section).^[25,27]

Furthermore, it should be noted that the particle count is proportional to the gas flow through the electrocatalytic cell, while it did not detectably vary with the potential that is applied to carry out the HER (Figure S3). Based on ICP-AES and BET results, one can hereby calculate an average K⁺ concentration on the surface of the catalysts of 0.2 K⁺/nm². Considering a K⁺ weight loading of 0.6% and the measured BET surface area of the Ni/SiO₂ samples (482.7 m²/g), one can calculate the average distribution of K⁺ on the catalyst surface. About 6 mg K⁺ ions are deposited per g of catalyst, which corresponds to roughly 12.4 µg/m², 0.3 µmol/m², 0.2 K⁺ atoms/nm² for catalysts 1, 5 and 6. Assuming hemispherical nickel metal nanoparticles of 1.2, 4.4 and 6.0 nm in diameter, this gives a nickel surface area of about 2.5, 30 and 57 nm² per particle, *i.e.*, 0.5 (implying about 1 K atom every two particles, on average), and 6 and 12 K⁺ atoms/particle, respectively. Considering 10 nickel atoms/nm², this gives a K:Ni surface atom ratio of 1/50. Accordingly, an effect on nickel activity at such low K/Ni ratios is consistent with results in literature on Ni(100) surfaces, for which CO and CO₂ methanation were affected starting from well-below Monolayer (ML) coverage (0.05 ML).^[28,29]

To benchmark the promotional effects that were reported in the literature, and those we have observed via *in situ* doping, K-doped Ni/SiO₂ catalyst samples 1–6 were prepared by

impregnation using a KOH solution, to achieve a loading of 0.6 wt% K (*i.e.* comparable to the amount of K⁺ deposited from the aerosol stream after 2 days). These samples will henceforth be called "*ex situ* doped" differentiated from the samples that are doped *in situ* via aerosol deposition. To prepare and simultaneously study *in situ* doped samples, a pure H₂ stream was bubbled through a saturator filled either with a 1 M KOH aqueous solution or with DI water.

To gain further insight into the nature of the (particle size dependent) effect of K on CO₂ methanation over nickel via both of these preparation methods, *operando* FT-IR spectroscopy was carried out at 400 °C for the sets of undoped (catalyst 1–6), *ex situ* doped samples (*ex situ* doped catalysts 1–6), and *in situ* doped (in situ catalysts 1–6). Catalyst sample 6 has very high nickel weight loading (60%) which makes the self-supported catalyst wafers of this sample needed to study FT-IR prone to breakage. The *ex-situ* catalyst preparation procedure apparently increased the fragility of this sample to an extent where it could not be studied in this setup.

Figure 4A shows the TOF trends as measured for the different samples. *Ex situ* doping has a clear deactivating effect, while *in situ* doping has a positive effect on the activity of Ni/SiO₂ catalysts in the methanation of CO₂ at 400 °C. Furthermore, it can be seen in Figure 4A and 4B that the initial doping effect of the aerosol is higher than when it reaches steady state. This was also observed in the all-in-one setup as described above, and shown in *e.g.* Figure 2. It is important to note that no clear particle size trend to the *in situ* promotion effects can be observed. While this appeared to be the case for the three particle sizes shown in Figure 3, the full set of catalyst samples tested here shows less of a distinctive trend. The general differences in promotion/deactivation trends, however, that are shown in Figure 4 are reflected in the FT-IR spectra, of which examples are shown in Figure 5. The supporting information shows the full set of FT-IR spectra in Figures S11 and S12. Figure 5 shows the region from 1400–2200 cm⁻¹ of the FT-IR spectra recorded during CO₂ hydrogenation at 400 °C for undoped, *in situ*, and *ex situ* doped catalyst samples 1, 4 and 5.

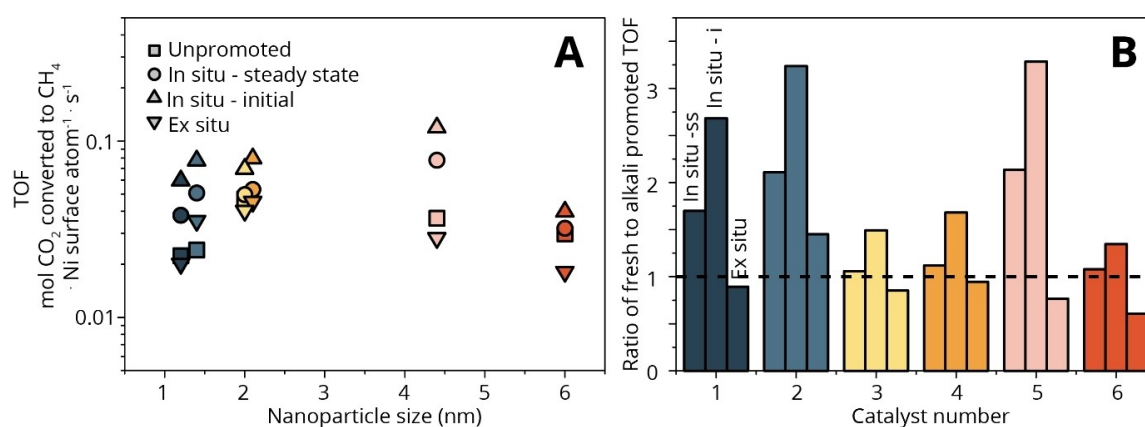


Figure 4. A) TOF trends for unpromoted, *ex situ* doped and *in situ* KOH promoted Ni/SiO₂ catalysts of different mean nickel particle sizes in CO₂ methanation at ambient pressure and 400 °C. The *in situ* promoted TOF trend is shown in its initial, and steady state. B) The promotional effect shown as a ratio of unpromoted versus various promoted states as displayed in A).

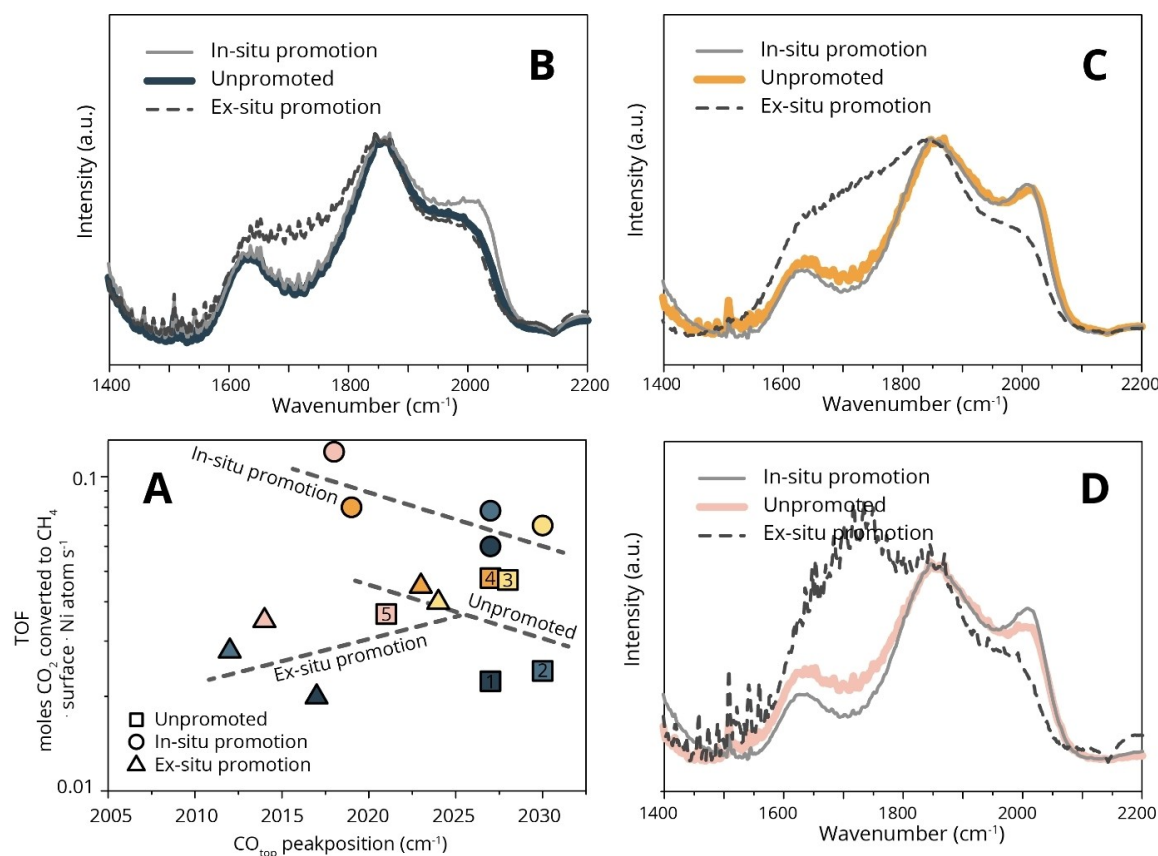


Figure 5. A) The TOF of Ni/SiO₂ catalysts of different mean nickel particle size in different states of KOH promotion (unpromoted, *in situ*, and *ex situ* doping) against the position of the peak maximum in *operando* FT-IR. The dotted lines are drawn as eye-guides, showing that with *in-situ* promotion the TOF increases but there is no significant change in the CO_{top} position, and with *ex-situ* promotion there is no significant increase in the TOF, but there is a significant change in the CO_{top} peak position. B–D) *Operando* FT-IR of the activity measurements shown in Figure 4, showing the catalysts of different mean nickel particle sizes B) catalyst 1, C) catalyst 4, D) catalyst 5) in undoped state, and doped *in situ* and *ex situ* with KOH. These spectra were baseline-subtracted and normalized to the peak at 1853 cm⁻¹.

In this region the CO stretching vibrations and also formate type species can be found, another important spectral feature which may be linked to the deactivating effect of *ex situ* doped catalysts.^[24,30]

Notably, *ex situ* doped samples show a lower relative intensity at around 2020 cm⁻¹, which ascribes to linearly adsorbed CO atop a single nickel atom^[31–34] and was shown to be an important descriptor for catalyst activity in Ni/SiO₂ in recent work.^[30] Deactivation is accompanied by the disappearance of the CO_(ads,top) signal with maximum at 2020 cm⁻¹. CO is an important intermediate in the formation of methane via the RWGS reaction. It is then subsequently converted to methane either via H-assisted CO dissociation or intermediate carbide hydrogenation. The binding strength, and coverage of CO is thus crucial in the formation of methane.^[24,30]

A trend in intensity of CO_{ads-top} can be observed in Figures 5A–C going from *in-situ* promoted > undoped > *ex-situ* doped catalysts. For the *in situ* promoted samples, this shift is much more subtle (if noticeable at all), while the change in activity is much more significant. Figures S13–S15 further show that no real trends can be ascribed to the effect of *in situ* doping on peak positions of CO_{ads} species. Notably, a higher

relative intensity of a broad feature around 1750 cm⁻¹, ascribed to carbonate species, is observed for the *ex situ* samples. The detectable presence of these species only in the *ex-situ* doped samples, and the fact that they are not hydrogenated to formate species, suggests that their formation could be due to K₂CO₃ formation over K deposits when exposed to air. In any case we can say that electronic effect of K on *ex-situ* doped Ni/SiO₂ seems to be more significant, which results in more back-donation to CO, thus effectively shifting the signal towards lower wavenumbers, which is in line with recent literature.^[21,22] The deactivating effect of K on Ni/SiO₂ is also shown in work by Campbell et al., in which K was only shown to deactivate Ni/SiO₂, even in very small amounts (0.05 wt.%).^[20,23] Yet, also here, the catalysts were preimpregnated with a K-containing solution, or prepared via co-impregnation. In fact, each of the catalyst samples where a deactivating effect was observed (Table S1), was treated with hydrogen at high temperature in the activation procedure of the catalyst. Also in our case, the *ex situ* doped samples were prepared in such a way that the K and nickel underwent a reduction procedure together. This reduction procedure in the presence of K has an obvious effect already on the particle size of some catalysts as could be seen

in the TEM analysis presented in Figure S9. This could be explained by an electronic interaction of K with Ni, or by the decomposition of KOH with temperature to yield K_2O and water at around $400\text{ }^\circ\text{C}$,^[35] which is known to affect Ni sintering.^[36] Another explanation could be the formation of bicarbonates after exposure to atmospheric CO_2 . Their decomposition to K_2CO_3 , CO_2 and water proceeds at low temperature ($100\text{--}200\text{ }^\circ\text{C}$).^[35] Poisoning via these strongly adsorbed species could inhibit the formation of product. During in-situ promotion, the reaction temperature is higher than the melting and decomposition temperature of KOH, which could explain why carbonates are not formed on the *in situ* doped catalysts (besides the low K concentration on the surface, as previously stated).

The effect of K on the activity could also be dependent on the K^+ distribution, as shown by recent observations in the coking resistance in catalytic methane steam reforming (the inverse reaction of CO_2 methanation) over Ni/Al_2O_3 catalysts.^[37] Yet no observable agglomeration could be found when the catalysts were examined by SEM-EDX (Figure S16). When examined by higher resolution STEM-EDX (Figure 6), there was also no observable difference in the comparison between the distribution of K throughout *ex situ* doped samples and *in situ* doped samples, which can be expected for such low amounts of K.

As no signs of agglomeration were detected by STEM-EDX and the *operando* FT-IR suggests a difference in electronic structure between *in situ* and *ex situ* doped samples, two plausible possibilities of the promotional effect of aerosols over *ex situ* promotion remain; first as already previously mentioned, alkali promoters are added to industrial methanation catalysts to suppress the formation of carbon deposits. The suppression of coke formation itself is not very relevant to our work as no

aromatic carbon vibrations (as aromatics are often considered as precursor molecules for coke deposit formation) could be observed in FT-IR for promoted or unpromoted reactions, and the promotional effect is larger initially than at steady state. The second possibility explaining the promotional effect of the *in situ* deposition of KOH via aerosols is a mechanism where the KOH promotes the removal of oxidizing species on the nickel surface via the formation of water. Both of these mechanisms require further investigation.

Conclusions

By combining *operando* FT-IR spectroscopy and a well-defined set of Ni/SiO_2 catalysts, we have shown both alkali promotion and poisoning of carbon dioxide hydrogenation over Ni/SiO_2 catalysts by KOH. *In situ* deposition of KOH-containing aerosols, realized by constructing an all-in-one setup capable of combining the H_2O electrolysis and CO_2 methanation steps, shows downstream promotion effects in the CO_2 methanation reaction. In contrast, the *ex situ* promotion of the Ni/SiO_2 catalysts with the same amount of KOH shows a deactivating effect for all catalyst samples under study. This deactivation can be rationalized in terms of the electronic effect of K in combination with the Sabatier principle, as *ex situ* promoted samples likely bind the reaction intermediate CO more strongly than is required. The mechanism for *in situ* promotion is either an increased rate in the hydrogenation of CH_x ($X=0\text{--}3$) fragments, or more facile water formation or desorption as the CO-containing reaction intermediates in FT-IR spectroscopy are unaffected by *in situ* promotion.

Practically this information translates to the application of a method of doping which is similar to dosing a certain amount of K via a H_2 feed coming directly from H_2O electrolysis in KOH electrolytes. In this way, the catalytic activity of nickel metal nanoparticles supported on SiO_2 in the Sabatier reaction can be efficiently enhanced. Although the mechanism as to what this can be attributed to requires further investigation, the work shows how a small amount of alkali promoters can dramatically change catalyst performance in CO_2 methanation.

Acknowledgements

B.M.W. thanks the Netherlands Organization for Scientific Research (NWO) Gravitation program, Netherlands Center for Multi-scale Catalytic Energy Conversion (MCEC), the Advanced Research Center Chemical Building Blocks Consortium (ARC CBBC) as well as NWO in the form of a joint TA-CHIPP grant with BASF for research funding. KX was funded by a NWO Earth and Life Science (ALW), under project number 824.14.002, grant to R.H..

Conflict of Interest

The authors declare no conflict of interest.

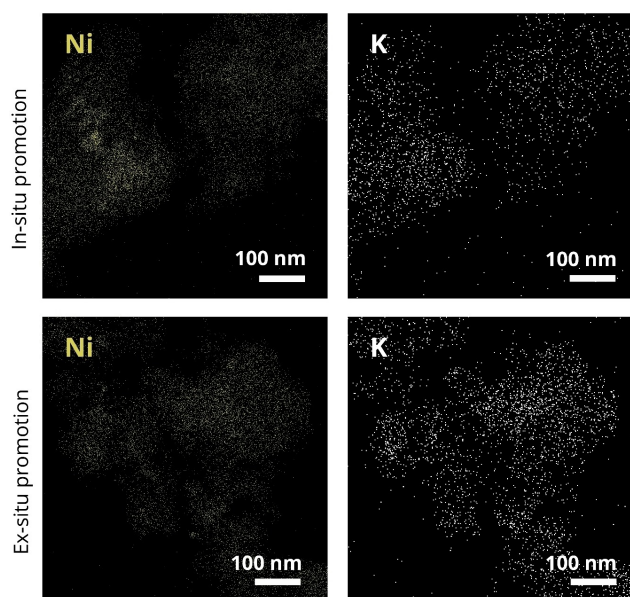


Figure 6. STEM-EDX maps of catalyst sample 5 (4.4 nm NiSiO_2) promoted *in situ* and *ex situ* with KOH.

Keywords: Power-to-methane · aerosol · alkali promotion · CO₂ hydrogenation · nickel

- [1] R. Schlögl, *Angew. Chem. Int. Ed.* **2015**, *54*, 4436–4439.
[2] R. Schlögl, *Angew. Chem. Int. Ed.* **2017**, *56*, 11019–11022.
[3] M. Götz, J. Lefebvre, F. Mörs, A. McDaniel Koch, F. Graf, S. Bajohr, R. Reimert, T. Kolb, *Renewable Energy* **2016**, *85*, 1371–1390.
[4] J. Kopyscinski, T. J. Schildhauer, S. M. A. Biollaz, *Fuel* **2010**, *89*, 1763–1783.
[5] H. Yang, C. Zhang, P. Gao, H. Wang, X. Li, L. Zhong, W. Wei, Y. Sun, *Catal. Sci. Technol.* **2017**, *7*, 4580–4598.
[6] C. Vogt, M. Monai, G. J. Kramer, B. M. Weckhuysen, *Nat. Cat.* **2019**, *2*, 188–197.
[7] S. Freni, N. Mondello, S. Cavallaro, G. Cacciola, V. N. Parmon, V. A. Sobyenin, *React. Kinet. Catal. Lett.* **2000**, *71*, 143–152.
[8] T. Haas, R. Krause, R. Weber, M. Demler, G. Schmid, *Nat. Cat.* **2018**, *1*, 32–39.
[9] *Handbook of Heterogeneous Catalysis*, 2nd Edition; Eds. G. Ertl, H. Knözinger, F. Schüth, J. Weitkamp, Wiley-VCH, Weinheim, **2008**.
[10] J.-B. Senderens, P. Sabatier, *C. R. Hebd. Seances Acad. Sci.* **1902**, *134*, 514–516.
[11] P. Sabatier, J.-B. Senderens, *C. R. Hebd. Seances Acad. Sci.* **1902**, *134*, 689–691.
[12] D. O. Hall, K. K. Rao, *Photosynthesis*, 6th Edition; Cambridge University Press, Cambridge, **1999**.
[13] AMES Reasearch Center, NASA, *Static Feed Water Electrolysis Module*, **1974**.
[14] Z. W. She, J. Kibsgaard, C. F. Dickens, I. Chorkendorff, J. K. Nørskov, T. F. Jaramillo, *Science* **2017**, *355*, eaad4998.
[15] C. P. Huang, J. T. Richardson, *J. Catal.* **1978**, *8*, 1–8.
[16] P. Schoubye, *J. Catal.* **1969**, *14*, 238–246.
[17] P. Panagiotopoulou, *Appl. Catal. B* **2018**, *236*, 162–170.
[18] A. Petala, P. Panagiotopoulou, *Appl. Catal. B* **2018**, *224*, 919–927.
[19] L. Xu, F. Wang, M. Chen, H. Yang, D. Nie, L. Qi, X. Lian, *RSC Adv.* **2017**, *7*, 18199–18210.
[20] G.-Y. Chai, J. L. Falconer, *J. Catal.* **1985**, *93*, 152–160.
[21] V. J. Cybulskis, J. Wang, J. H. Pazmiño, F. H. Ribeiro, W. N. Delgass, *J. Catal.* **2016**, *339*, 163–172.
[22] B. Liang, H. Duan, X. Su, X. Chen, Y. Huang, X. Chen, J. J. Delgado, T. Zhang, *Catal. Today* **2017**, *281*, 319–326.
[23] T. K. Campbell, J. L. Falconer, *Appl. Catal.* **1989**, *50*, 189–197.
[24] C. Vogt, E. Groeneveld, G. Kamsma, M. Nachtegaal, L. Lu, C. J. Kiely, P. H. Berben, F. Meirer, B. M. Weckhuysen, *Nat. Cat.* **2018**, *1*, 127–134.
[25] Y. Kim, H. Sievering, J. Boatman, D. Wellman, A. Pszeny, *J. Geophys. Res.* **1995**, *100*, 23027.
[26] Q. Yin, C. L. Hill, *Nat. Chem.* **2017**, *10*, 6–7.
[27] D. W. Cooper, D. W. Underhill, M. J. Ellenbecker, *Am. Ind. Hyg. Assoc. J.* **1979**, *40*, 365–371.
[28] C. T. Campbell, D. W. Goodman, *Surf. Sci.* **1982**, *123*, 413–426.
[29] D. E. Peebles, D. W. Goodman, J. M. White, *J. Phys. Chem.* **1983**, *87*, 4378–4387.
[30] C. Vogt, E. B. Sterk, M. Monai, J. Palle, A. E. M. Melcherts, B. Zijlstra, E. Groeneveld, P. H. Berben, J. M. Boereboom, E. J. M. Hensen, F. Meirer, I. A. W. Filot, B. M. Weckhuysen, *Nat. Commun.* **2019**, *10*, 5330.
[31] J. C. Campuzano, R. G. Greenler, *Surf. Sci.* **1979**, *83*, 301–312.
[32] S. B. Mohsin, M. Trenary, H. J. Robota, *J. Phys. Chem.* **1988**, *92*, 5229–5233.
[33] K. A. Layman, M. E. Bussell, *J. Phys. Chem. B* **2004**, *108*, 10930–10941.
[34] M. Courtois, S. J. Teichner, *J. Catal.* **1962**, *135*, 121–135.
[35] R. L. Lehman, J. S. Gentry, N. G. Glumac, *Thermochim. Acta* **1998**, *316*, 1–9.
[36] J. Zieliński, *Catal. Lett.* **1992**, *12*, 389–393.
[37] T. Borowiecki, A. Denis, M. Rawski, A. Gołębiowski, K. Stołcki, J. Dmytryk, A. Kotarba, *Appl. Surf. Sci.* **2014**, *300*, 191–200.

Manuscript received: February 25, 2020
Accepted manuscript online: March 1, 2020
Version of record online: April 1, 2020